Kamal Selvam
Laboratoire Ondes et Milieux Complexes,
CNRS & Université Le Havre Normandie,
Le Havre 76600, France

Emir Öngüner
Department of Aerodynamic and
Fluid Mechanics,
BTU Cottbus–Senftenberg,
Cottbus 03046, Germany

Jorge Peixinho[1]
Laboratoire Ondes et Milieux Complexes,
CNRS & Université Le Havre Normandie,
Le Havre 76600, France
e-mail: jorge.peixinho@univ-lehavre.fr

El-Sayed Zanoun
Department of Aerodynamics and
Fluid Mechanics,
BTU Cottbus–Senftenber,
Cottbus 03046, Germany;
Benha Faculty of Engineering,
Benha University,
Benha 13512, Egypt

Christoph Egbers
Department of Aerodynamics and
Fluid Mechanics,
BTU Cottbus–Senftenberg,
Cottbus 03046, Germany

Wall Pressure in Developing Turbulent Pipe Flows

Velocity fluctuations are widely used to identify the behavior of developing turbulent flows. The pressure on the other hand, which is strongly coupled with the gradient of the mean velocity and fluctuations, is less explored. In this study, we report the results of wall pressure measurements for the development of pipe flow at high Reynolds numbers along the axial direction. It is found that the pressure fluctuations increase exponentially along the pipe with a self-similarity scaling. The exponential growth of the pressure fluctuations along the pipe saturates after reaching a critical position around 50 diameters from the inlet. It qualitatively agrees with the critical position usually adopted for fully developed turbulence, which was obtained from earlier velocity fluctuations at various locations along the pipe centerline. Results also show that the exponential growth of the pressure fluctuations is weakly affected by the presence of ring obstacles placed close to the pipe inlet. Finally, it is found that the pressure fluctuations decrease as a function of Reynolds number, contrary to the boundary layer flow. [DOI: 10.1115/1.4039294]

1 Introduction

Linear stability theory [1–6] suggests that the perturbations at the inlet of pipes are responsible for transition to turbulence at Reynolds number roughly around 10,000. Here, the Reynolds number is defined as $\mathrm{Re} = UD/\nu$, where U is the mean velocity, D is the pipe diameter, and ν is the kinematic viscosity of the fluid. To achieve laminar flow, the perturbations like background vorticity or thermal gradients at the inlet could be minimized using honeycombs, screens, and temperature control. Several experimental observations [7–17] have shown that the laminar state in pipe flows can be achieved over a wide range of flow rates [11] or Reynolds number up to 100,000. Furthermore, direct numerical simulations of spatially developing pipe flows have also been carried out, showing the existence of helical vortex filament and large-scale vortices, which grow exponentially with the axial distance as they are convected downstream and developed into turbulence [18]. The question that arises is what is the critical axial position where the turbulent flow becomes fully developed? Fully developed turbulence usually means that the statistics of the flow properties (velocity and pressure) indicate invariant behavior in the axial direction downstream the critical position.

The entry flow does have a significant role in all experimental investigations of developing turbulence in a pipe. Background vorticity or thermal gradients from the reservoir can be carried into the pipe by the flow [12]. These effects can be minimized using honeycombs and screens. The shape of the inlet can also induce disturbances and wind tunnels use specifically designed bell-mouth contractions to avoid flow separation that appear in sharp-edged entry [10,12,13]. Many pipe flows of engineering interest have both with sharp entry and disturbed flow at the inlet, these flows have received some attention in experimental investigations [9,19]. When making comparison with theoretical or numerical works, a well-defined contraction is necessary. Measurements of the statistics of centerline velocity fluctuations (root-mean-square (RMS) and high-order moments) were used to obtain the axial position for getting fully developed pipe turbulence [12,16,20–22]. According to Zagarola and Smits [21] and Zanoun et al. [16], most of the transition to turbulence occurs in the entrance region up to about 60 diameters from the pipe inlet. Yet, most of the literature on developing turbulent flow has been conducted using velocity fluctuations, whereas pressure fluctuations are less explored.

The entrance region deserves to be studied in detail as a transition from inlet flow to fully developed turbulence is taking place. First, the boundary layer is developing and, second, the turbulent structures are growing. Mean and fluctuation velocity profiles in the entrance region are similar in laminar and turbulent flow [12]. Hence, it is difficult to apprehend the effects of turbulence vortex growth and boundary layer growth. It is believed that new data on wall pressure fluctuations combined to velocity data at various positions along the pipe will help to clarify the location of the transition. A direct application of this research may be used to optimize flow control in the entrance region. For instance, modern strategies use actuators like plasma actuators or vortex generators [23]. In the present study, the flow is tripped using ring obstacles of different heights from the pipe wall in order to investigate the behavior of pressure fluctuations in a developing turbulent circular pipe flow. The pressure field of an incompressible flow can be

[1]Corresponding author.

Contributed by the Fluids Engineering Division of ASME for publication in the Journal of Fluids Engineering. Manuscript received August 21, 2017; final manuscript received December 15, 2017; published online March 29, 2018. Assoc. Editor: Sergio Pirozzoli.

obtained by taking the divergence of the Navier–Stokes equation. This gives Poisson equation, which shows a strong coupling between pressure and velocity

$$\frac{1}{\rho}\nabla^2 P = -\frac{\partial U_i}{\partial x_j}\frac{\partial U_j}{\partial x_i} \tag{1}$$

where the pressure $P = \overline{p} + p'$, the velocity $U_i = \overline{u}_i + u_i'$, $U_j = \overline{u}_j + u_j'$, and ρ is the fluid density. Hence, decomposing Eq. (1) results in the following pressure fluctuation equation:

$$\frac{1}{\rho}\nabla^2 p' = -2\frac{\partial^2}{\partial x_i \partial x_j}\left(u_i'\overline{u}_j\right) - \frac{\partial^2}{\partial x_i \partial x_j}\left(u_i'u_i' - \overline{u_i'u_j'}\right) \tag{2}$$

The right-hand side in Eq. (2) contains two terms. The first term represents the interaction between the gradient of the mean velocity field and the gradient of the turbulent velocity field. The second term represents turbulence-turbulence interaction. This clearly shows a link between the mean velocity gradient, the velocity fluctuations, the pressure fluctuations, and how they redistribute the turbulence between various fluctuating components.

The goal of the present investigation is to measure the pressure along the pipe for a wide range of Reynolds numbers and locate the critical position where the flow becomes fully developed. In the first part, the experiment and the wall pressure measurement system are briefly described. In the second part, the results for the wall mean and fluctuating pressure are discussed. Then, the effect of the ring obstacles is presented. Finally, the scaling of the pressure fluctuation as a function of Reynolds number is addressed.

2 Experimental Setup

The Cottbus large pipe (CoLaPipe) test facility has a diameter of $D = 190 \pm 0.3$ mm, length of 26 m ($137D$) long and was constructed from 13 acrylic sections of 2 m long each and 5 mm thick. The sections were initially aligned using laser and assembled using flanges, bolts, and nuts. Figure 1(*a*) presents a schematic of the pipe test section. The airflow is driven using a radial blower of 45 kW. Before entering the pipe, air flow passes through a cooling system to maintain constant temperature. All the experiments were conducted at $20 \pm 1\,^{\circ}$C. Before the inlet of the pipe test section, air flows through a settling chamber that was setup with a perforated plate, honeycomb, and screens of different mesh sizes to damp flow fluctuations ahead of reaching the measuring positions [12,14]. Moreover, a smooth inlet contraction section is used, designed using a fifth-order polynomial. Bernoulli's equation is used to calculate Reynolds number by using the mean pressure values obtained before and after the contraction section in the constant section part. At the exit of the contraction, the streamwise turbulence intensity is less than 0.5%. The experimental setup has a working range of $6 \times 10^4 < \mathrm{Re} < 10^6$ (5–80 m/s). It corresponds to $0.3 < u_\tau < 3$ m/s, where u_τ is the friction velocity in fully developed flow: $u_\tau = \sqrt{\tau_w/\rho}$, and τ_w is the wall shear stress, which is estimated from the mean pressure drop, Δp, over a length, L, between two pressure taps along the pipe away from pipe inlet where the flow is fully developed as $\tau_w = D\Delta p/4L$. More details about the facility can be found in König et al. [24] and König [25].

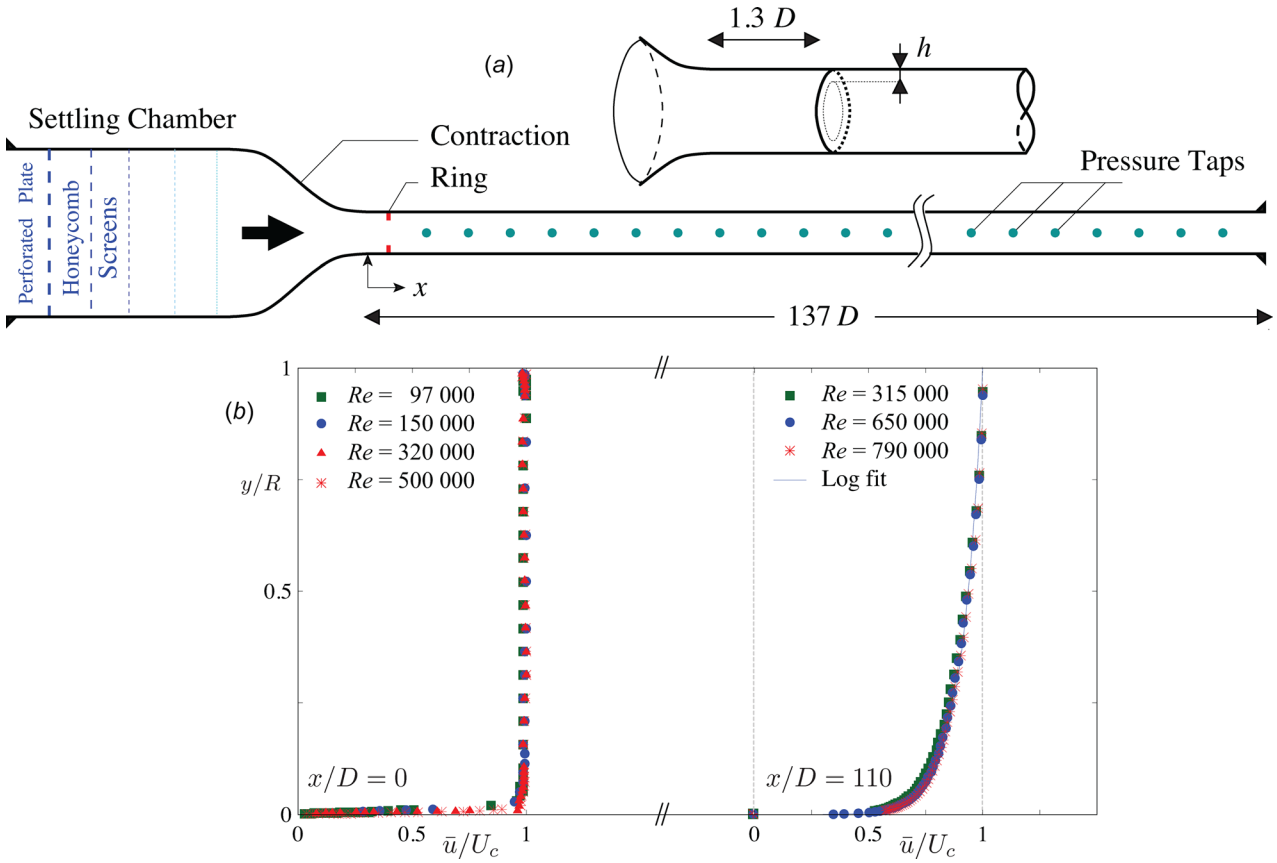

Fig. 1 (*a*) **Schematic of the pipe test section. The inset shows a detailed view of the ring perturbation. (*b*) Mean velocity profiles normalized by the centerline velocity, U_c, at the inlet ($x/D = 0$) and downstream at $x/D = 110$ for different Reynolds numbers. The velocity profiles at $x/D = 110$ are fitted with a log law fit: $\overline{u}/U_c = 0.092\ln(y/R)+1.0$, where U_c is the centerline mean velocity, y the position from the wall, and R the radius of the pipe.**

2.1 Natural Transition and Ring Obstacles at the Inlet. Figure 1(*b*) shows velocity profiles normalized by the centerline velocity, U_c, at the inlet ($x/D = 0$) and downstream at $x/D = 110$ for different Re obtained using hot wire anemometer [24] when no obstacle is present. The inlet, $x = 0$, corresponds to the onset of the constant diameter section. At the inlet, the mean axial velocity profile is almost flat and, downstream, reaches the well-known fully developed turbulent profiles [16,21]. The measured velocity profiles in Fig. 1(*b*) at $x/D = 110$ are fitted using the classical log law velocity profile.

In the previous turbulence studies [20,26], the pipe flows are tripped close to the inlet and the measurements are conducted at various downstream positions to assure that the flow is turbulent. Here, one ring was located at $1.3D$ from the inlet (see the inset of Fig. 1(*a*)), slightly away from the exit of the contraction, where the flow uniformity exists, as shown in Fig. 1(*b*), and is used to estimate the mean flow velocity, U. Each ring is made out of 2-mm-thick aluminum plate. The inner radius of the ring is at a constant height, h, from the pipe wall. The natural transition corresponds to $h = 0$ and the perturbed cases correspond to $h = 4.5$, 9.5, 15.5, and 21.5 mm, which correspond to area blockage of 10, 20, 30, and 40%, respectively.

2.2 Wall Pressure Measurement System. The wall pressure along the pipe test section is measured using wall pinholes and static pressure taps. The pinhole diameter, d, is 400 μm and its depth, ℓ, is $\approx$1.0 mm. Hence, the pinhole aspect ratio is $\ell/d \approx 2.5$. The normalized pinhole diameter, $d^+ = du_\tau/\nu$, lies within the range $10 \leq d^+ \leq 65$, depending on the current working range, $2650 \leq \mathrm{Re}_\tau \leq 15,000$, where Re_τ is the friction Reynolds number defined as $\mathrm{Re}_\tau = \mathrm{R}u_\tau/\nu$ with R being the pipe radius. According to Shaw [27], the error estimated in the present wall pressure measurements due to the pinhole size effect is minimal, i.e., $\Pi = \delta p/\tau_w \leq 0.2$, where Π is the nondimensional pressure error. Short flexible tubes have been used connecting pressure taps to the pressure measuring device to avoid the damping effect of long tubes. Pressure taps are available along the pipe test section on 41 locations. At each location, three pressure taps are installed 120 deg around the pipe circumference. The pressure is measured using piezo-electric transducer (Measurement Systems, model 9116) mounted behind the pinhole. All pressure measurements are taken using a pressure scanner with a range of 7 kPa, connected through an ethernet cable to a computer. The pressure transducer is calibrated to compensate transducer outputs for offset, sensitivity, nonlinearity, and thermal effects. The transducer has a frequency response up to 500 Hz with measurement resolution of $\pm 0.003\%$ full scale. Five to ten pressure taps are simultaneously measured and the acquisition is performed using LabView. After the signals are recorded, a new series of taps is measured until the desired number of pressure points along the pipe is recorded. The data are then postprocessed using MATLAB. Each pressure signal is 10,000 samples at a frequency of 100 Hz. Initially, 50,000 samples were acquired to determine the pressure fluctuations. With 10,000 samples, we found a deviation of the fluctuations about 1.2%.

3 Results and Discussion

The results mainly consist of pressure measurements along the pipe. The first set of results is obtained for a pipe without ring disturbance. The second set of results presents the effect of ring disturbances on pressure measurements and the scaling of pressure for a wide range of Reynolds number.

3.1 Friction Factor for Developed Turbulent Pipe Flow. To validate the experiment, the friction factor, $\lambda = 8\tau_w/\rho U^2$, as a function of the Reynolds number is measured in the fully developed region and is shown in Fig. 2(*a*). λ was calculated by five points averaging using pressure data in the region $70 < x/D < 130$. In Fig. 2(*a*), the variation of λ versus Re using the skin friction formula proposed by Blasius [28] is also shown

$$\lambda = 0.3164/\mathrm{Re}^{1/4} \tag{3}$$

which is considered to be valid only for $\mathrm{Re} \leq 100,000$. Note that the present turbulent experimental data are much higher than the Hagen–Poiseuille law for laminar flow: $\lambda = 64/\mathrm{Re}$, also presented in Fig. 2(*a*). The error bars in Fig. 2 represent the dispersion in the measurements based on five rehearsals, so 9.6% confidence interval on Re and 5.6% on λ. The friction factor relationship with the Reynolds number, proposed by Prandtl, was obtained from the integration of the mean velocity profile [21] and can be written as

$$1/\lambda^{1/2} = C_1 \log(\mathrm{Re}\lambda^{1/2}) + C_2 \tag{4}$$

where C_1 and C_2 are coefficients, which may or may not depend on Re. When $C_1 = 2.0$ and $C_2 = -0.8$, then Eq. (4) is identical to

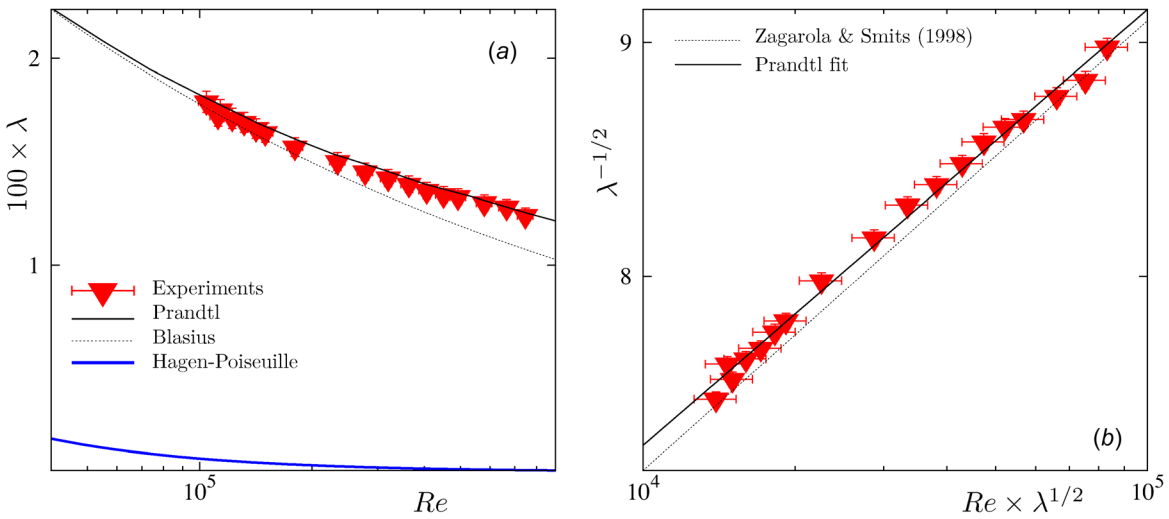

Fig. 2 Friction factor, λ, in fully developed turbulent flow. (*a*) λ as a function of Re. The lines represent the Hagen–Poiseuille (laminar), the Prandtl, and the Blasius laws described in the text. (*b*) $\lambda^{-1/2}$ as a function of $\mathrm{Re}\times\lambda^{1/2}$. The bottom line is the Prandtl fit for Ref. [21] smooth pipe data and the top line is a fit to the present experiments.

that by Prandtl for the smooth-pipe data of Nikuradse [29]. In Fig. 2(*b*), a least-squares approximation was used on our data to calculate the values for the coefficients: $C_1 = 2.0$ and $C_2 = -0.18$. The reasoning for the coefficients in Eq. (4) being independent of the Reynolds number assumes (i) the existence of a log law up to the centerline and (ii) the average velocity to be insensitive to the near-wall region thickness [21].

3.2 Pressure Fluctuations Along the Pipe

3.2.1 Pressure Fluctuations Without Ring Disturbance. The facility allows for measurements of the wall static pressure: $P = \overline{p} + p'$, where $\overline{p}$ is the mean pressure and p' is the fluctuation. Figure 3(*a*) shows the mean pressure difference as a function of the axial position, x/D. The reference pressure, $\overline{p}_e$, here is at $x/D = 100$, so that $\overline{p}_e = \overline{p}_{x=100D}$. It decreases monotonously from the inlet and the slope depends on the Reynolds number, because there is a strong pressure gradient driving the flow. The mean pressure, $\overline{p}$, does not convey any information about the position for the transition to fully developed turbulence. However, irregular behavior around $30 < x/D < 60$ for the high Reynolds cases seems to indicate changes in slope, which may be the region where turbulent spots are initiated. Hence, the behavior of fluctuations, p', should be explored. Experimentally, p' is the RMS of the pressure. Figure 3(*b*) presents the pressure fluctuations, p', along the pipe and for different Reynolds numbers. Here, p' is normalized by pressure difference along the contraction, Δp, the reference pressure of the experiment used to calculate the Reynolds number. At the inlet, $p'/\Delta p$ is small and increases with the axial position before reaching a steady-state value, corresponding to fully developed turbulence. Again, in the region $30 < x/D < 60$, there seems to be an irregular behavior before reaching the steady-state, which may be associated with the region where turbulent spots and hairpin vortex form and develop [18].

To investigate this self-similar growth, different normalizations can be implemented [30]. In Fig. 3(*c*), p'^+ is shown as a function of x/D, where $p'^+ = p'/\rho u_\tau^2$ and $u_\tau^2 = \lambda U^2/8$ is the friction velocity from the fully developed turbulent region. Only a partial collapse of the data is observed and the most striking observation is the exponential increase of the pressure fluctuations close to the inlet region. This is in a good agreement with the exponential growth of the total kinetic energy of the flow in the simulations of Wu et al. [18] in developing turbulent pipe flow. The p'^+ data can be fitted using an exponential equation: $p'^+ = \alpha - \beta \exp(-\gamma x/D)$, where α, β, and γ are positive constants. Note that this simple fit already introduces three constants from which physical meaning is hard to assess.

Further, one can normalize the data using the asymptotic value of the exponential, $p'^+_\infty = \alpha$, as shown in Fig. 3(*d*). The measurement and the associated fits indicate that the curvature of the exponential growth seems to shift toward low x/D for large Reynolds number. This corresponds to the decrease of the parameter γ with Re. The decrease of the distance for saturated pressure fluctuations is in qualitative agreement with the experiments of Zanoun

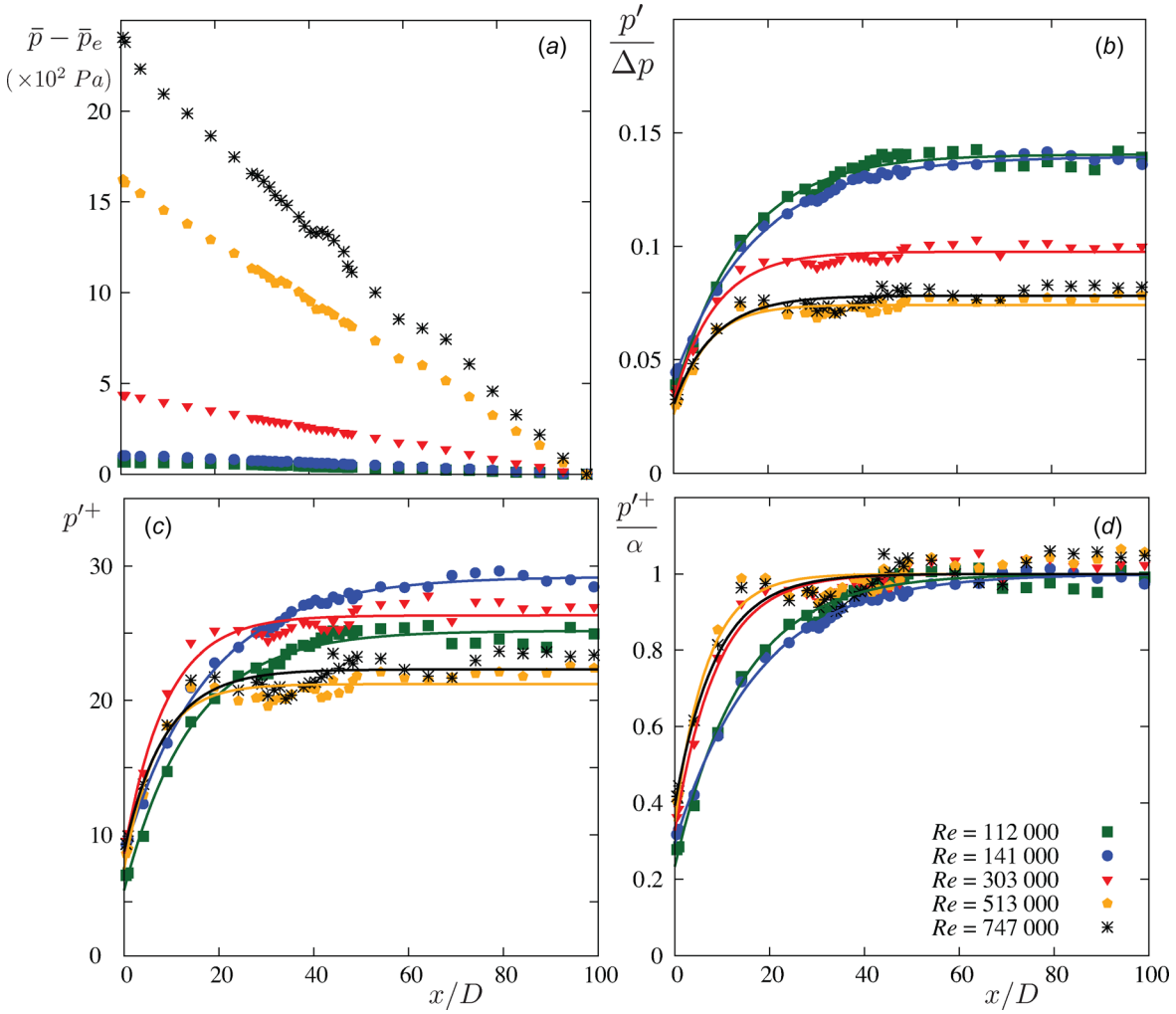

Fig. 3 Wall mean pressure and fluctuations along the pipe without ring: (*a*) $\overline{p} - \overline{p}_e$, (*b*) $p'/\Delta p$, (*c*) p'^+, and (*d*) p'^+/α versus x/D for different Reynolds numbers

et al. [16] and Zanoun and Egbers [31] that found an abrupt decrease of the critical position for fully developed turbulence as the Reynolds number increases. Their procedure to obtain the critical axial position was relying on measuring the statistical moments of the centerline velocity at different axial positions. At the critical position, the skewness and the kurtosis or flatness present peaks before reaching constant/asymptotic values. The present pressure measurements seem to indicate a shorter critical entrance length than the centerline velocity data, presumably because the pressure measurements were carried out at the wall dealing with mean and RMS pressure data. A quantitative characterization requires, however, a complete study aiming at measuring high-order moments of pressure signals which is beyond the scope of this work.

3.2.2 Pressure Fluctuations With Ring Perturbation. The question arises, how the exponential growth of the pressure fluctuations along the pipe was robust to obstacles. Figure 4 presents the wall pressure fluctuations along the pipe for different Reynolds numbers and each plot corresponds to a case where a ring perturbation is placed at $1.3D$ from the inlet. Note that the Reynolds number changes due to the blockage effect. The ring was located slightly away from the exit of the contraction, where the flow uniformity exists and is used to estimate the bulk flow velocity, U. Each ring corresponds to an obstruction area of 10, 20, 30, and 40% of the pipe cross section, as sketched in the insets of Fig. 4. It has a strong effect locally, which can be quantified through a sudden p' peak at $x/D = 1.3$ to 8, corresponding to a flow separation region and represented as shaded areas in Figs. 4(*c*) and 4(*d*). However, downstream ($x/D > 10$) the pressure evolves exponentially as in the case without perturbation. This local effect is also observed for bluff bodies placed in the center of the pipe [32]. The normalized pressure has similar exponential growth behavior as in the case of flow without ring disturbance. Note that the exponential fit is a simplified representation of p', owing to the fact that the flow now involves many length scales and the effect of the ring. The results with a ring (Fig. 4) indicate a small but systematic increase of $p'/\Delta p$ when compared to the unperturbed flow (Fig. 3(*b*)) and specifically for high blockages larger than 20% (Figs. 4(*c*)–4(*d*)). This is in agreement with the experiments of Pollard et al. [33] for $\mathrm{Re} = 180,000$, who found 1 to 2% increase in wall pressure with the use of ring manipulators.

To study the effect of ring disturbances, one representative flow velocity in the middle of our working range was chosen and Fig. 5 shows the pressure fluctuations evolution for different ring disturbances for $\mathrm{Re} \simeq 300,000$. The points represent the experimental measurements and the lines are exponential fits to the data. The scaling using α from the exponential fitting proposed earlier leads to a good overlap in the downstream region of the pipe. Again, the exponential fit is an oversimplified representation, as it does not

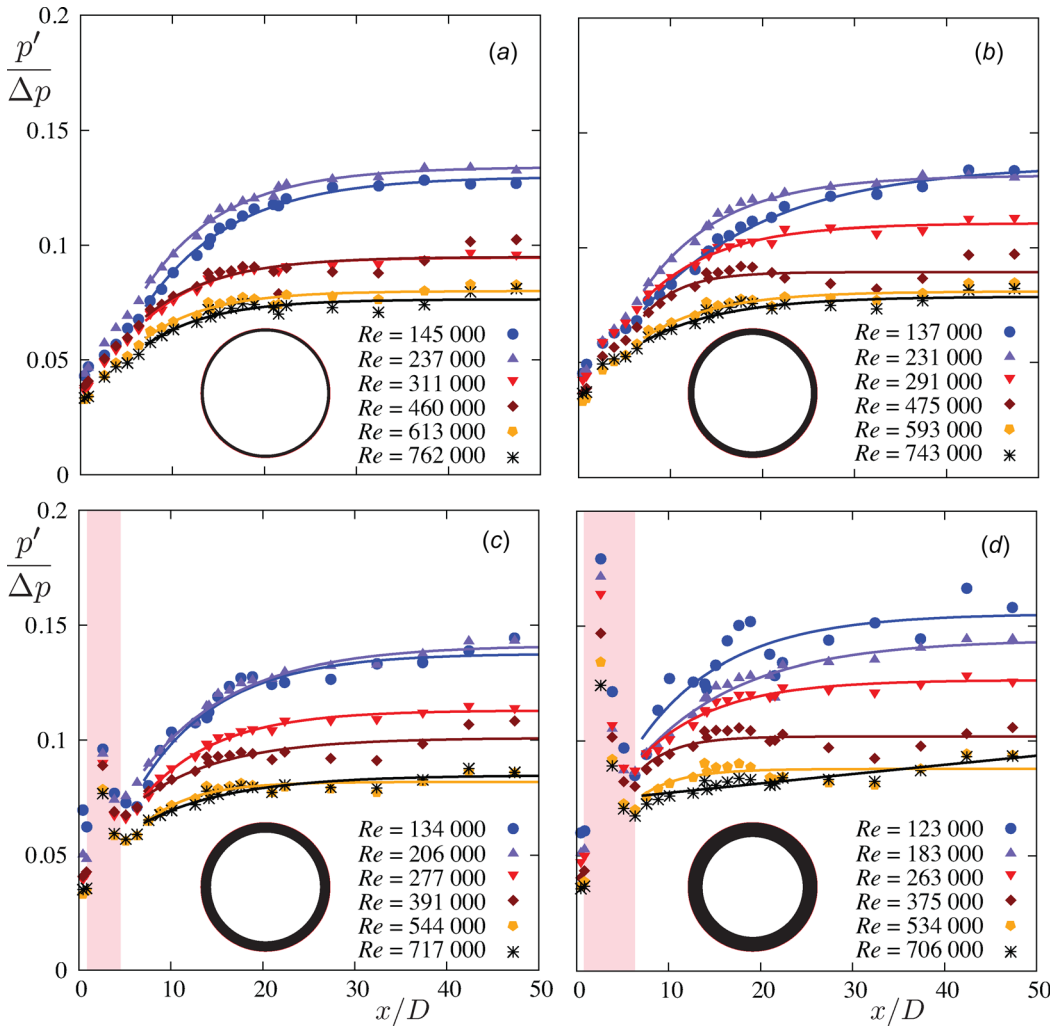

Fig. 4 Wall pressure fluctuations, $p'/\Delta p$, along the pipe, x/D, for different Re with ring perturbations at $1.3D$ from the inlet. The perturbation makes a area obstruction of (*a*) 10, (*b*) 20, (*c*) 30, and (*d*) 40%. The insets are sketches of the ring obstruction. The shaded area marks the position of local effects of the rings.

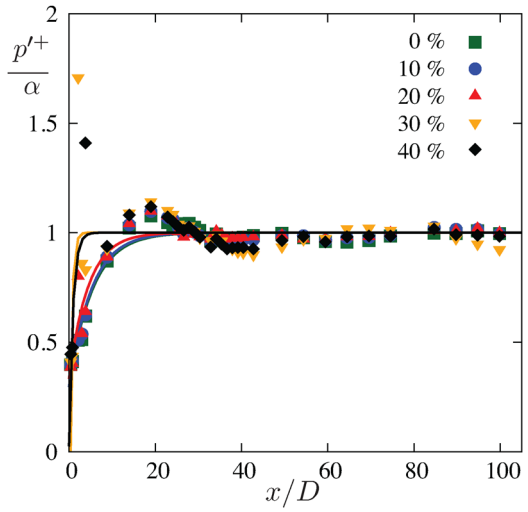

Fig. 5 Wall pressure fluctuations at Re $\simeq$ 300,000 along the pipe for different ring disturbances. The lines are exponential fits.

take into account the effect of the ring. However, the local effect of the ring has a strong influence on the position of saturation. Yet, it can be seen that without ring disturbance, i.e., 0% disturbance, the position of saturation of the fit is $x/D \approx 50$, whereas in the case of 20% disturbance, the position of saturation shifts upstream at $x/D \approx 34$. Similarly, applying a higher ring disturbance, 40% (black line), the point of saturation shifts upstream. It seems that the application of ring disturbance to the incoming flow initiates turbulence much earlier upstream and leads to fully developed turbulence, which in turn saturates the pressure fluctuations.

3.3 Scaling of Wall Pressure Fluctuations. In this section, the behavior of the pressure fluctuations in fully developed turbulence flow is analyzed. This is the region where p' saturated. In Fig. 6, we present the variation of pressure fluctuations as a function of Re for different perturbation cases. Here, p' is an average of three points in the saturated region around $x/D = 50$. Figure 6(*a*) is based on a scaling using integral flow parameters and clearly shows that $p'/\Delta p$ decreases as a function of the Reynolds number. Another representation of these data can be achieved using local scaling parameters such as u_τ. The pressure fluctuation, p', is normalized by ρu_τ^2, as shown in Fig. 6(*b*) as a function of Re_τ, where Re_τ is Ru_τ/ν, with R being the radius of the pipe. The lines are power law fit with an exponent of -0.15 ± 0.05. One might conclude from the data that the fully developed turbulent flow downstream is independent of the ring perturbation. The decrease in the pressure fluctuation seems surprising when compared to the turbulent boundary layer flow [30,34–37] that increases. In pipe flow, the curved surface of the pipe interior contributes to the interchange of counter-rotating vortices toward the pipe core, strongly influencing the flow structure in the inner region as well as in the core of the pipe flow [38]. The scaling cannot hold for large Reynolds numbers when compressibility effect arises. For the 40% blockage, the maximum achievable throat velocity was 73 m/s, which corresponds to 0.21 in terms of Mach number and weak compressibility effects. Except in the high speed with large blockage, most of the measurements presented here are not affected by compressibility effects. In the case of large speed and 40% blockage, some noise could be heard, which is assumed to be due to massive turbulent separation behind the ring obstacles that provide sound radiation. The previous works have measured the spectra of single location pressure signals [39–44] in order to quantify sound production, acoustic effects, compressible effects, and vibroacoustic response.

4 Conclusions

The behavior of pressure was studied in a developing turbulent pipe flow. Both mean pressure measurements and pressure fluctuations were discussed in detail. It was observed that the pressure fluctuations have an initial exponential growth along the pipe with axial position, before reaching a constant value. In the development region, the pressure fluctuations increase suggesting energy growth at the same time as the mean velocity profile is developing. The constant pressure fluctuation region corresponds to developed turbulent flow that is always observed for x/D above 30.

The critical position for transition was observed to move upstream up to 50 when the Reynolds number is increased up to 700,000. Moreover, the use of rings at the inlet also shortens the transition length. For rings with blockage area larger than 20%, a peak of pressure fluctuation was observed downstream of the contraction exit, corresponding to turbulent separation followed by reattachment.

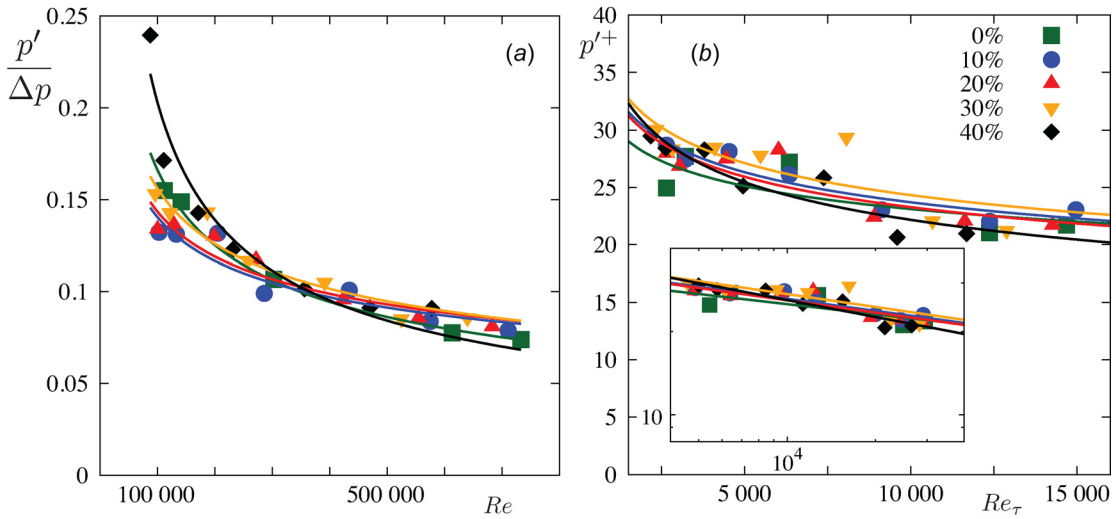

Fig. 6 Wall pressure fluctuations as a function of the Reynolds number in the saturated region for different ring disturbances. (*a*) $p'/\Delta p$ versus Re and (*b*) p'^+ versus Re_τ in linear scale. The inset is also p'^+ versus Re_τ in log scale.

The root-mean-square values of the wall pressure normalized by the inner variables are found to be decreasing as a function of the Reynolds number. This is in contrast to the behavior of pressure fluctuations measured on a flat plate boundary layer. The curved surface of the pipe and the confinement contribute to the interchange of counter-rotating vortices toward the pipe core, which strongly influence the flow structure in the inner region of pipe flow.

In the near future, further measurements will be carried using wall hot wire and hot film to verify Eq. (2) on the interaction between the mean velocity field and the gradient of the turbulent velocity fluctuations close to the wall.

Acknowledgment

K.S. is grateful to the financial support of the region Normandie. C.E. and E.Ö. acknowledge financial support from DFG FOR1182 research group "Turbulence."

Funding Data

- European High-Performance Infrastructures in Turbulence (EuHIT) program.
- CNRS LIA ISTROF.

References

[1] Tatsumi, T., 1952, "Stability of the Laminar Inlet-Flow Prior to the Formation of Poiseuille Regime, II," J. Phys. Soc. Jpn., **7**(5), pp. 495–502.

[2] Huang, L. M., and Chen, T. S., 1974, "Stability of Developing Pipe Flow Subjected to Non-Axisymmetric Disturbances," J. Fluid Mech., **63**(1), pp. 183–193.

[3] Sarpkaya, T., 1975, "A Note on the Stability of Developing Laminar Pipe Flow Subjected to Axisymmetric and Non-Axisymmetric Disturbances," J. Fluid Mech., **68**(2), pp. 345–351.

[4] Gupta, S. C., and Garg, V. K., 1981, "Effect of Velocity Distribution on the Stability of Developing Flow in a Pipe," Phys. Fluids, **24**(4), pp. 576–578.

[5] Da Silva, D. F., and Moss, E. A., 1994, "The Stability of Pipe Entrance Flows Subjected to Axisymmetric Disturbances," ASME J. Fluids Eng., **116**(1), pp. 61–65.

[6] Sahu, K. C., and Govindarajan, R., 2007, "Linear Instability of Entry Flow in a Pipe," ASME J. Fluids Eng., **129**(10), pp. 1277–1280.

[7] Reynolds, O., 1883, "An Experimental Investigation of the Circumstances Which Determine Whether the Motion of Water Shall Be Direct or Sinuous, and of the Law of Resistance in Parallel Channels," Proc. R. Soc. London, **35**(224–226), pp. 84–99.

[8] Ekman, V. W., 1910, "On the Change From Steady to Turbulent Motion of Liquids," Ark. Mat. Astron. Fys., **6**, pp. 1–16.

[9] Comolet, R., 1950, "Recherche Sur La Genèse De La Turbulence Dans Les Conduites En Charge," Ph.D. thesis, Public Science and Technology Ministry of Air, Paris, France.

[10] Lindgren, E. R., 1957, "The Transition Process and Other Phenomena in Viscous Flow," Ark. Fys., **12**, pp. 1–169.

[11] Pfenninger, W., 1961, "Boundary Layer Suction Experiments With Laminar Flow at High Reynolds Numbers in the Inlet Length of a Tube by Various Suction Methods," *Boundary Layer and Flow Control*, G. V. Lachman, ed., Pergamon Press, New York, pp. 961–980.

[12] Wygnanski, I. J., and Champagne, F. H., 1973, "On Transition in a Pipe—Part 1: The Origin of Puffs and Slugs and the Flow in a Turbulent Slug," J. Fluid Mech., **59**(2), pp. 281–335.

[13] Draad, A. A., Kuiken, G. D. C., and Nieuwstadt, F. T. M., 1998, "Laminar–Turbulent Transition in Pipe Flow for Newtonian and Non-Newtonian Fluids," J. Fluid Mech., **377**, pp. 267–312.

[14] Durst, F., Ray, S., Ünsal, B., and Bayoumi, O. A., 2005, "The Development Lengths of Laminar Pipe and Channel Flows," ASME J. Fluids Eng., **127**(6), pp. 1154–1160.

[15] Peixinho, J., and Mullin, T., 2007, "Finite-Amplitude Thresholds for Transition in Pipe Flow," J. Fluid Mech., **582**, pp. 169–178.

[16] Zanoun, E.-S., Kito, M., and Egbers, C., 2009, "A Study on Flow Transition and Development in Circular and Rectangular Ducts," ASME J. Fluids Eng., **131**(6), p. 061204.

[17] Mullin, T., 2011, "Experimental Studies of Transition to Turbulence in a Pipe," Annu. Rev. Fluid Mech., **43**(1), pp. 1–24.

[18] Wu, X., Moin, P., Adrian, R. J., and Baltzer, J. R., 2015, "Osborne Reynolds Pipe Flow: Direct Simulation From Laminar Through Gradual Transition to Fully Developed Turbulence," Proc. Natl. Acad. Sci. U. S. A., **112**(26), pp. 7920–7924.

[19] Ghajar, A. J., and Tam, L.-M., 1994, "Heat Transfer Measurements and Correlations in the Transition Region for a Circular Tube With Three Different Inlet Configurations," Exp. Therm. Fluid Sci., **8**(1), pp. 79–90.

[20] Laufer, J., 1954, "The Structure of Turbulence in Fully Developed Pipe Flow," National Advisory Committee for Aeronautics, Washington, DC, Technical Report No. 1174.

[21] Zagarola, M. V., and Smits, A. J., 1998, "Mean-Flow Scaling of Turbulent Pipe Flow," J. Fluid Mech., **373**, pp. 33–79.

[22] Furuichi, N., Terao, Y., Wada, Y., and Tsuji, Y., 2015, "Friction Factor and Mean Velocity Profile for Pipe Flow at High Reynolds Numbers," Phys. Fluids, **27**(9), p. 095108.

[23] Habchi, C., Russeil, S., Bougeard, D., Harion, J.-L., Lemenand, T., Della Valle, D., and Peerhossaini, H., 2012, "Enhancing Heat Transfer in Vortex Generator-Type Multifunctional Heat Exchangers," Appl. Therm. Eng., **38**, pp. 14–25.

[24] König, F., Zanoun, E.-S., Öngüner, E., and Egbers, C., 2014, "The CoLaPipe—the New Cottbus Large Pipe Test Facility at Brandenburg University of Technology Cottbus-Senftenberg," Rev. Sci. Instrum., **85**(7), p. 075115.

[25] König, F., 2015, "Investigations of High Reynolds Number Pipe Flow," Ph.D. thesis, Brandenburgische Technische Universität Cottbus-Senftenberg, Cottbus, Germany.

[26] Perry, A. E., and Abell, C. J., 1975, "Scaling Laws for Pipe-Flow Turbulence," J. Fluid Mech., **67**(2), pp. 257–271.

[27] Shaw, R., 1960, "The Influence of Hole Dimensions on Static Pressure Measurements," J. Fluid Mech., **7**(4), pp. 550–564.

[28] Blasius, H., 1908, "Boundary Layer in Fluids With Little Friction," Z. Math. Phys., **56**, pp. 1–37.

[29] Nikuradse, J., 1933, "Strömungsgesetze in Rauen Rohren," VDI Forschungsheft, Berlin, Technical Report No. 361.

[30] Tsuji, Y., Fransson, J. H. M., Alfredsson, P. H., and Johansson, A. V., 2007, "Pressure Statistics and Their Scaling in High-Reynolds-Number Turbulent Boundary Layers," J. Fluid Mech., **585**, pp. 1–40.

[31] Zanoun, E.-S., and Egbers, C., 2016, "Flow Transition and Development in Pipe Facilities," J. Eng. Appl. Sci., **63**(2), pp. 141–159.

[32] Venugopal, A., Agrawal, A., and Prabhu, S. V., 2017, "Investigations on Bluff Bodies as Improved Vortex Shedders Placed Inside a Circular Pipe," ASME J. Fluids Eng., **139**(4), p. 041204.

[33] Pollard, A., Savill, A. M., and Thomann, H., 1989, "Turbulent Pipe Flow Manipulation: Some Experimental and Computational Results for Single Manipulator Rings," Appl. Sci. Res., **46**(3), pp. 281–290.

[34] Kraichnan, R. H., 1956, "Pressure Fluctuations in Turbulent Flow Over a Flat Plate," J. Acoust. Soc. Am., **28**(3), pp. 378–390.

[35] Corcos, G. M., 1964, "The Structure of the Turbulent Pressure Field in Boundary-Layer Flows," J. Fluid Mech., **18**(3), pp. 353–378.

[36] Schlatter, P., and Örlü, R., 2012, "Turbulent Boundary Layers at Moderate Reynolds Numbers: Inflow Length and Tripping Effects," J. Fluid Mech., **710**, pp. 5–34.

[37] Naka, Y., Stanislas, M., Foucaut, J.-M., Coudert, S., Laval, J.-P., and Obi, S., 2015, "Space–Time Pressure–Velocity Correlations in a Turbulent Boundary Layer," J. Fluid Mech., **771**, pp. 624–675.

[38] Wei, T., and Willmarth, W. W., 1989, "Reynolds-Number Effects on the Structure of a Turbulent Channel Flow," J. Fluid Mech., **204**(1), pp. 57–95.

[39] Clinch, J. M., 1969, "Measurements of the Wall Pressure Field at the Surface of a Smooth-Walled Pipe Containing Turbulent Water Flow," J. Sound Vib., **9**(3), pp. 398–419.

[40] Farabee, T. M., and Casarella, M. J., 1991, "Spectral Features of Wall Pressure Fluctuations Beneath Turbulent Boundary Layers," Phys. Fluids, **3**(10), pp. 2410–2420.

[41] Agarwal, N. K., 1994, "The Sound Field in Fully Developed Turbulent Pipe Flow Due to Internal Flow Separation—Part I: Wall-Pressure Fluctuations," J. Sound Vib., **169**(1), pp. 89–109.

[42] Browne, L. W. B., and Dinkelacker, A., 1995, "Turbulent Pipe Flow: Pressures and Velocities," Fluid Dyn. Res., **15**(3), pp. 177–204.

[43] Durant, C., Robert, G., Filippi, P. J. T., and Mattei, P.-O., 2000, "Vibroacoustic Response of a Thin Cylindrical Shell Excited by a Turbulent Internal Flow: Comparison Between Numerical Prediction and Experimentation," J. Sound Vib., **229**(5), pp. 1115–1155.

[44] Borisyuk, A. O., 2010, "Experimental Study of Wall Pressure Fluctuations in Rigid and Elastic Pipes Behind an Axisymmetric Narrowing," J. Fluids Struct., **26**(4), pp. 658–674.